Evaluation of Three Lattice Boltzmann Models for Particulate Flows

Liang Wang[1], Zhaoli Guo[1,*], Baochang Shi[2] and Chuguang Zheng[1]

[1] *State Key Laboratory of Coal Combustion, Huazhong University of Science and Technology, Wuhan, 430074, P.R. China.*
[2] *School of Mathematics and Statistics, Huazhong University of Science and Technology, Wuhan, 430074, P.R. China.*

Abstract. A comparative study is conducted to evaluate three types of lattice Boltzmann equation (LBE) models for fluid flows with finite-sized particles, including the lattice Bhatnagar-Gross-Krook (BGK) model, the model proposed by Ladd [Ladd AJC, *J. Fluid Mech.*, 271, 285-310 (1994); Ladd AJC, *J. Fluid Mech.*, 271, 311-339 (1994)], and the multiple-relaxation-time (MRT) model. The sedimentation of a circular particle in a two-dimensional infinite channel under gravity is used as the first test problem. The numerical results of the three LBE schemes are compared with the theoretical results and existing data. It is found that all of the three LBE schemes yield reasonable results in general, although the BGK scheme and Ladd's scheme give some deviations in some cases. Our results also show that the MRT scheme can achieve a better numerical stability than the other two schemes. Regarding the computational efficiency, it is found that the BGK scheme is the most superior one, while the other two schemes are nearly identical. We also observe that the MRT scheme can unequivocally reduce the viscosity dependence of the wall correction factor in the simulations, which reveals the superior robustness of the MRT scheme. The superiority of the MRT scheme over the other two schemes is also confirmed by the simulation of the sedimentation of an elliptical particle.

PACS: 44.05.+e, 47.11.-j, 47.56.+r

Key words: Lattice Boltzmann equation, finite-sized particles, numerical performance, sedimentation in channel.

1 Introduction

Particulate flows occur widely in both industrial and scientific applications, such as river sediment resuspension and transport, blood clogging and cell transport in arteries and

---

Corresponding author. Email addresses: zlguo@hust.edu.cn (Z. Guo), wlsa0612@gmail.com (L. Wang), shibc@hust.edu.cn (B. Shi), cgzheng@mail.hust.edu.cn (C. Zheng)

veins, DNA and polymer molecules [1, 2], colloidal suspensions, etc. Owing to the importance of these applications, experimental and numerical studies have been attracting considerable attention in the past decades.

In particulate flows, the fluid phase can be well-described by the Navier-Stokes (NS) equations, while the description of the particle phase can be classified into two categories, i.e., the point-particle method and the finite-size particle method. In the point-particle method, a solid particle is considered as a mass point with negligible size and shape, and its position and velocity are traced in a Lagrangian manner. The interactions between fluid and particles are modeled by some empirical or semi-empirical relations. The point-particle method is suitable for most engineering applications with a large number of particles with sizes far smaller than the flow length scale. However, the point-particle method is not enough to reveal the fundamental mechanism of the fluid-particle interactions. In contrast, the size and shape of a particle are considered in the finite-size particle method, and the particle-fluid interactions can be described through the no-slip boundary conditions on the particle interface directly. Therefore, this method can be viewed as a direct numerical simulation method for particulate flows. Several direct numerical simulation methods, including the finite element method (FEM) and the finite volume method (FVM), have been developed within this framework [3–6]. However, these methods usually suffer from expensive computational costs due to frequent remeshing and projection in simulations of particulate flows.

Besides these conventional methods that solve the NS equations, the lattice Boltzmann equation (LBE), which is a method based on kinetic theory, has also been applied to particulate flows [7–16]. The first application of LBE to particulate flows with finite-sized particles is attributed to Ladd [10, 11]. In this method [10, 11], a fixed regular grid system is used to represent the flow field and the solid particle. A modified bounce-back rule [11] is proposed to treat the no-slip boundary condition on the particle-fluid interface, and an approach based on momentum exchange is developed to calculate the hydrodynamic force exerting on the solid particle. It is assumed that the fluid can pass through the boundary of the suspended solid particle and occupy its interior domains. In this way, both the interior and exterior fluid nodes can be treated in an identical manner as the particle moves on the lattice. It is noted that in Ladd's model the particle behaves like a rigid one with the combined mass and moment of inertia of the shell plus the internal fluid. Consequently, when the density ratio of particle to fluid is close to or smaller than unity, numerical instability will occur in the particle update procedure [16–18]. To overcome this limit, a number of methods have been developed to partially or fully remove the internal fluid of particle [12, 13, 19].

Another problem of Ladd's model is that the particle surface is represented by the boundary nodes which are actually a set of points located at the middle of the link between a fluid node and a solid node. This arrangement means that the body surface is approximated by a stair-step shape. As the particle moves, this will generate some noisy forces and further bring fluctuations to the particle velocities. Some improvements [20–23] have been proposed for more accurate representation of the particle shape

with curved boundary condition.

More recently, a number of approaches that combined LBE with other types of methods were also developed for fluid-particle systems. For instances, Ten Cate et al. [24] introduced an adaptive-forcing method into LBE, and Owen et al. [25] established a computational framework that hydrodynamically combined LBE with the discrete element method (DEM) for suspensions, while Kollmannsberger et al. [26] proposed a partitioned approach to couple LBE and FEM for fluid-structure problems. With the LBE and DEM, Feng et al. [27,28] simulated some turbulent fluid- particle flows. Feng and Michaelides proposed a method to incorporate the immersed boundary method (IBM) [29,30] into the LBE through either a penalty approach [31] or a direct-forcing method [32]. However, as pointed out in Refs. [17,32,33], *a priori* selection of the stiffness coefficient is needed for a specific problem [31], and the NS equations are solved by a finite difference method to determine the density force, which may spoil the merits of LBE and bring errors to the force computations on the object [32]. In addition, it is observed that some leakage of fluid momentum inside the solid particle emerges in some cases. Some improved LBE methods [17,33,34] were proposed recently, and some combinations of LBE with other methods were also developed [35–39].

Although a variety of LBE methods have been developed for particulate flows [10,16, 33,40,41], the criterion for model selection is still not clear in practical applications, and a systematic investigation of the performances of these schemes is still desirable. In the present work, we intend to conduct a detailed comparison of the most widely used LBE schemes by simulating the sedimentation of a particle in a 2D infinite channel in terms of the accuracy, numerical stability, computational efficiency, and robustness.

The remainder of this paper is organized as follows. Section 2 presents a brief introduction of the three LBE schemes, including the lattice BGK (LBGK) scheme, Ladd's scheme, and the multiple-relaxation-time (MRT) scheme. Section 3 provides the results of this study. The test case of the sedimentation of one particle in an infinite channel is first briefly described, and then the numerical results obtained by the three LBE schemes are compared with the analytical results and the existing reference data. A detailed assessment of the three LBE schemes, which focus on the accuracy, numerical stability, computational efficiency and the viscosity dependence of the wall correction factor, is also included in this section. To confirm the findings, Section 4 presents a further comparison of the three LBE schemes by simulating the sedimentation of an elliptical particle in an infinite channel. A brief summary is presented in Section 5 finally.

2 The lattice Boltzmann method for particulate flows

2.1 General formulation

In LBE for particulate flows, the fluid motion is described as:

$$f_i(\boldsymbol{x}+\boldsymbol{c}_i\delta_t,t+\delta_t)-f_i(\boldsymbol{x},t)=\Omega_i(\boldsymbol{x},t), \tag{2.1}$$

where $f_i(x,t)$ is the fluid distribution function (DF) for the particle with discrete velocity c_i at time t and position x, δ_t is the time increment, and $\Omega_i(x,t)$ is the collision term. The fluid density ρ and velocity u are defined by the zeroth and first velocity moments of the DF:

$$\rho=\sum_i f_i, \qquad \rho u=\sum_i c_i f_i. \tag{2.2}$$

In the typical D2Q9 model [42,43], the discrete velocity set is

$$c_i=\begin{cases} (\,0,0), & i=0, \\ \left(\cos\left[(i-1)\pi/2\right],\sin\left[(i-1)\pi/2\right]\right)c, & i=1-4, \\ \left(\cos\left[(i-1)\pi/2+\pi/4\right],\sin\left[(i-1)\pi/2+\pi/4\right]\right)\sqrt{2}\,c, & i=5-8, \end{cases} \tag{2.3}$$

where $c=\delta_x/\delta_t$ is the lattice speed, and δ_x is the lattice constant.

In practice, the evolution of Eq. (2.1) is usually decomposed into two steps:

$$\text{Collision}: \quad f_i^*(x,t)=f_i(x,t)+\Omega_i(x,t), \tag{2.4a}$$
$$\text{Streaming}: \quad f_i(x+c_i\delta_t,t+\delta_t)=f_i^*(x,t). \tag{2.4b}$$

where $f_i^*(x,t)$ denotes the post-collision state of DF. Within the LBE framework, the collision models in Eq. (2.1) are usually based on the linearized collision operator. According to the collision models, most LBE models for simulating particulate flows can be classified into three categories: the BGK scheme, Ladd's scheme, and the MRT scheme.

2.1.1　BGK scheme

In the BGK scheme, the collision operator is approximated by a relaxation process:

$$\Omega_i(x,t)=-\frac{1}{\tau}\left[f_i(x,t)-f_i^{(eq)}(x,t)\right], \tag{2.5}$$

where $f_i^{(eq)}(x,t)$ is the local equilibrium distribution function (EDF), and τ is the dimensionless relaxation time which characterizes the rate of approaching to equilibrium.

The EDF for the D2Q9 model has the following form:

$$f_i^{(eq)}=\omega_i\rho\left[1+\frac{c_i\cdot u}{c_s^2}+\frac{(c_i\cdot u)^2}{2c_s^4}-\frac{u^2}{2c_s^2}\right], \tag{2.6}$$

where ω_i is the weighting factor which is given as follows: $\omega_0=4/9$, $\omega_i=1/9$ for $i=1,2,3,4$, and $\omega_i=1/36$ for $i=5,6,7,8$. $c_s=c/\sqrt{3}$ is the sound speed. In the low Mach number limit, the macroscopic NS equations with a kinematic viscosity $\nu=c_s^2(\tau-\frac{1}{2})\delta_t$ can be recovered from the LBE through the Chapman-Enskog expansion.

2.1.2 Ladd's scheme

In Ladd's scheme [10,16], in addition to the mass density ρ and velocity $\boldsymbol{u}$, the momentum flux $\boldsymbol{\Pi}$ is also involved, which is defined as:

$$\boldsymbol{\Pi} = \sum_i \boldsymbol{c}_i \boldsymbol{c}_i f_i. \tag{2.7}$$

The equilibrium momentum flux can be obtained by

$$\boldsymbol{\Pi}^{eq} = \sum_i \boldsymbol{c}_i \boldsymbol{c}_i f_i^{(eq)} = c_s^2 \rho \boldsymbol{I} + \rho \boldsymbol{u}\boldsymbol{u}.$$

The post-collision distribution in Ladd's scheme is written as a series of the moments

$$f_i^* = \omega_i \left[\rho + \frac{\rho \boldsymbol{u} \cdot \boldsymbol{c}_i}{c_s^2} + \frac{(\rho \boldsymbol{u}\boldsymbol{u} + \boldsymbol{\Pi}^{neq,*}) : (\boldsymbol{c}_i \boldsymbol{c}_i - c_s^2 \boldsymbol{I})}{2c_s^4} \right]. \tag{2.8}$$

The relaxation of the non-equilibrium momentum flux $\boldsymbol{\Pi}^{neq}$ is realized as follows:

$$\boldsymbol{\Pi}^{neq,*} = (1+\lambda_\nu)\overline{\boldsymbol{\Pi}}^{neq} + \frac{1}{3}(1+\lambda_\zeta)\left(\boldsymbol{\Pi}^{neq} : \boldsymbol{I}\right)\boldsymbol{I}, \tag{2.9}$$

where $\boldsymbol{\Pi}^{neq} = \sum_i \boldsymbol{c}_i \boldsymbol{c}_i f_i^{neq} = \boldsymbol{\Pi} - \boldsymbol{\Pi}^{eq}$, and $\overline{\boldsymbol{\Pi}}^{neq} = \overline{\boldsymbol{\Pi}} - \overline{\boldsymbol{\Pi}}^{eq}$ (the overline used here indicates the traceless projection). The parameters λ_ν and λ_ζ are the eigenvalues of the linearized collision operator and are related to the shear and bulk viscosities, respectively.

In the original formulation of Ladd's model [10, 16], the collision operator has three parameters which respectively allow for separate relaxation of three kinds of modes, i.e. shear modes, bulk modes, and kinetic modes. The kinetic modes can also have an effect on the post-collision distributions, but the eigenvalues corresponding to these modes are set to -1 in Ladd's scheme so that they are "killed". Through a multi-scale analysis [16,44], the NS equations can be recovered in the limit of low Mach number, in which the shear and bulk viscosities are determined respectively by

$$\nu = -c_s^2 \delta_t \left(\frac{1}{\lambda_\nu} + \frac{1}{2}\right), \qquad \zeta = -\frac{2c_s^2}{3}\delta_t \left(\frac{1}{\lambda_\zeta} + \frac{1}{2}\right). \tag{2.10}$$

2.1.3 MRT scheme

The MRT collision model can be written as

$$\Omega_i(\boldsymbol{x},t) = -\sum_j \Phi_{ij}\left(f_j(\boldsymbol{x},t) - f_j^{(eq)}(\boldsymbol{x},t)\right), \tag{2.11}$$

where Φ_{ij} is the component of a collision matrix $\boldsymbol{\Phi}$. In moment space, the MRT collision model can be expressed as:

$$\Omega(\boldsymbol{x},t) = -\boldsymbol{M}^{-1}\boldsymbol{S}\left[\boldsymbol{m}(\boldsymbol{x},t) - \boldsymbol{m}^{(eq)}(\boldsymbol{x},t)\right], \tag{2.12}$$

where m and $m^{(eq)}$ are the moment vector and the corresponding equilibria in moment space, respectively. M is the transformation matrix that maps the distribution functions to their moments,

$$m = M \cdot f, \qquad f = M^{-1} \cdot m.$$

In Eq. (2.12) $S = M\Phi M^{-1}$ is the corresponding collision matrix in moment space, which is a diagonal matrix of relaxation rates $\{s_i\}$: $S = diag(s_0, s_1, \cdots, s_8)$. For the D2Q9 model, the transformation matrix M can be obtained by the Gram-Schmidt orthogonalization procedure [45], which can be found in [45–48].

With this transformation matrix, the moment vector can be expressed as,

$$m = (\rho, \, e, \, \varepsilon, \, j_x, \, q_x, \, j_y, \, q_y, \, p_{xx}, \, p_{xy})^T,$$

where T denotes the transpose operator. In the vector m, ρ is the fluid density, e and ε are related to the total energy and the energy square, j_x and j_y are components of the momentum, i.e., $j_x = \rho u_x$, $j_y = \rho u_y$, q_x and q_y are the x and y components of the energy flux, and p_{xx} and p_{xy} are related to the symmetric and traceless components of the stress tensor, respectively.

The corresponding equilibria of the moments are given by

$$m^{(eq)} = (\rho, \, e^{(eq)}, \, \varepsilon^{(eq)}, \, j_x, \, q_x^{(eq)}, \, j_y, \, q_y^{(eq)}, \, p_{xx}^{(eq)}, \, p_{xy}^{(eq)})^T, \tag{2.13}$$

where the density ρ and the momentum $j = \rho u$ are the conserved moments. The equilibria of the non-conserved moments depend on the conserved moments [45]:

$$e^{(eq)} = \rho(-2 + 3u_x^2 + 3u_y^2), \qquad \varepsilon^{(eq)} = -\rho(-1 + 3u_x^2 + 3u_y^2), \tag{2.14a}$$

$$q_x^{(eq)} = -\rho u_x, \qquad q_y^{(eq)} = -\rho u_y, \tag{2.14b}$$

$$p_{xx}^{(eq)} = \rho(u_x^2 - u_y^2), \qquad p_{xy}^{(eq)} = \rho u_x u_y. \tag{2.14c}$$

Noticing that the relaxation rates s_0, s_3 and s_5 are related to the conserved moments and can take any values, which are set to be zero in the present work. The other relaxation rates are chosen in the range $0 < s_i < 2$ to satisfy the stability condition for non-conserved moments [45].

For the above D2Q9 model, the shear viscosity ν and the bulk viscosity ζ are given by

$$\nu = c_s^2 \left(\frac{1}{s_7} - \frac{1}{2} \right) \delta_t, \qquad \zeta = c_s^2 \left(\frac{1}{s_1} - \frac{1}{2} \right) \delta_t. \tag{2.15}$$

In addition, it is required that $s_7 = s_8$ and $s_4 = s_6$.

In MRT-LBE, the collision step is first implemented in the moment space, and then transformed back to the velocity space,

$$m^*(x,t) = m(x,t) - S\left[m(x,t) - m^{(eq)}(x,t)\right], \qquad f^* = M^{-1}m^*. \tag{2.16}$$

It is noted that the three LBE schemes have close relations. If we set all the relaxation rates s_i to be $1/\tau$, the MRT-LBE scheme reduces to the standard LBGK scheme, while if we set $s_7 = s_8 = -1/\lambda_\nu$, $s_1 = 6\lambda_\zeta/(\lambda_\zeta - 4)$, and $s_i = 1$ for other moments, the MRT-LBE scheme reduces to Ladd's scheme. Ladd's scheme is also equivalent to the LBGK scheme with $\tau = 1$ in the special case of $\lambda_\nu = \lambda_\zeta = -1$. For convenience, we will set $s_7 = s_8 = 1/\tau$ in the MRT-LBE scheme and $\lambda_\nu = -1/\tau$ in Ladd's scheme.

2.2 Particle-fluid boundary conditions

In order to apply the LBE to particulate flows, two issues should be carefully considered. One is how to treat the boundary conditions on a particle surface, and the other is how to calculate the hydrodynamic forces exerted on the solid particle. In this work, we will follow Ladd's method [10, 16] to treat a particle, of which the interior is also filled with the fluid. It is noteworthy that such treatment can ensure the mass and momentum conservation of the flow, and can also facilitate the computations. The particle surface is approximated by some boundary nodes, as illustrated in Fig. 1, which are placed halfway along the links between the fluid node and solid node. The boundary condition imposed at the solid-fluid interface is the no-slip condition, i.e., at a boundary node x_b the fluid velocity u_b is set to be

$$u_b = U_p + \Omega_p \times (x_b - R), \tag{2.17}$$

where U_p and Ω_p are the particle translational and angular velocities, respectively, R is the location of the mass center of the particle.
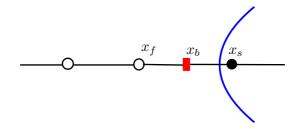

Figure 1: Schematic of the location of boundary nodes. Solid circle: solid node; Open circle: fluid node; Solid square: boundary node which is placed halfway along the links of fluid and solid nodes.

In order to realize the no-slip condition for a moving particle, Ladd [10, 11] proposed a modified bounce-back rule in which the boundary velocity is taken into account,

$$f_{i'}(x, t+\delta_t) = f_i^*(x, t) - 2\omega_i \rho \frac{c_i \cdot u_b}{c_s^2}, \tag{2.18}$$

where x is the position of the node adjacent to the solid surface, i' denotes the opposite direction of the incident direction i (reflection direction). In the original scheme [10, 11], Ladd applied the above rule to the boundary nodes on both sides of the solid surface. Such bounce-back rule will be employed in the present work.

At the boundary node x_b, the hydrodynamic force exerted on the solid particle along c_i can be calculated by the momentum exchange method, which is written as

$$F_i(x_b,t) = 2\frac{\delta_x^2}{\delta_t}c_i\left[f_i^*(x,t) - 2\omega_i\rho\frac{c_i \cdot u_b}{c_s^2}\right]. \tag{2.19}$$

The total force F_t and torque T_t on the solid particle can be determined by,

$$F_t = \sum_{x_b}\sum_i F_i(x_b), \qquad T_t = \sum_{x_b}\sum_i (x_b - R) \times F_i(x_b), \tag{2.20}$$

where the summation runs over all boundary nodes and all relevant directions for each boundary node.

The motion and rotation of the particle can be determined from the following equations:

$$M_p\frac{dU_p}{dt} = F_t, \qquad I_p\frac{d\Omega_p}{dt} = T_t, \tag{2.21}$$

where M_p and I_p are the mass and the moment of inertia of the particle, respectively. In the numerical scheme for solving these two equations, we adopt the following formula to update both the translational and rational velocities of the particle at each time:

$$U_p^{n+1} = U_p^n + \delta_t F_t / M_p, \tag{2.22}$$

and

$$\Omega_p^{n+1} = \Omega_p^n + \delta_t T_t / I_p. \tag{2.23}$$

The particle is updated by integrating the velocity after each time step.

2.3 Particle-particle and particle-wall interactions

When a large number of particles exist in a container, it is possible that one particle locates very close to another or the wall under certain circumstances. If the distance is less than one lattice, the above force calculation will break down because no sufficient nodes exist for implementing the momentum exchange. In addition, it is unphysical that the particles penetrate into each other's boundary or into the wall. To resolve these problems, we can add some short-range repulsive forces when the minimum gap of the particle-particle or particle-wall is less than a given threshold. In this paper, we will adopt the collision model proposed by Wan and Turek [49]. For particle-particle collisions, the repulsive force is given by

$$F_{i,j}^p = \begin{cases} 0, & d_{i,j} > R_i + R_j + \xi, \\ \frac{1}{\varepsilon_p'}(X_i - X_j)(R_i + R_j - d_{i,j}), & d_{i,j} \leqslant R_i + R_j, \\ \frac{1}{\varepsilon_p}(X_i - X_j)(R_i + R_j + \xi - d_{i,j})^2, & R_i + R_j \leqslant d_{i,j} \leqslant R_i + R_j + \xi, \end{cases} \tag{2.24}$$
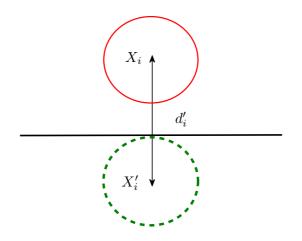
Figure 2: Schematic diagram of the location of the imaginary particle.

where R_i and R_j are the radii of the ith and jth particles, $\boldsymbol{X}_i$ and $\boldsymbol{X}_j$ are their centers, $d_{i,j} = |\boldsymbol{X}_i - \boldsymbol{X}_j|$ is the distance between the centers, ξ is the threshold which is set to be one lattice spacing in the present work, ε'_p and ε_p are two small positive stiffness parameters for particle-particle collisions and both are set to be 1.0×10^{-7}. Similarly, for the particle-wall collisions, the repulsive force is given by

$$\boldsymbol{F}_i^w = \begin{cases} 0, & d'_i > 2R_i + \xi, \\ \frac{1}{\varepsilon'_w}(\boldsymbol{X}_i - \boldsymbol{X}'_i)(2R_i - d'_i), & d'_i \leqslant 2R_i, \\ \frac{1}{\varepsilon_w}(\boldsymbol{X}_i - \boldsymbol{X}'_i)(2R_i + \xi - d'_i)^2, & 2R_i \leqslant d'_i \leqslant 2R_i + \xi, \end{cases} \tag{2.25}$$

where $\boldsymbol{X}'_i$ is the coordinate vector of the center of the nearest imaginary particle located on the boundary and $d'_i = |\boldsymbol{X}_i - \boldsymbol{X}'_i|$ (see Fig. 2), ε'_w and ε_w are two stiffness parameters which are set to be $\varepsilon'_w = \varepsilon'_p/2$ and $\varepsilon_w = \varepsilon_p/2$ in the calculations. It should be pointed out that the supplementary force of particle collision, $\boldsymbol{F}_i^{col} = \boldsymbol{F}_{i,j}^p + \boldsymbol{F}_i^w$, is regarded as an external force added to the total force acting on the i-th particle.

3   Numerical results and discussions for circular particle

In this section, we intend to compare the performance of the three LBE schemes in terms of accuracy, numerical stability, computational efficiency, and robustness. The test problem is the sedimentation of a circular particle under gravity in an infinite channel, as sketched in Fig. 3. The diameter of the particle is D, and the size of the channel is $W \times H$, where W and H are width and height of the channel, respectively. The gravitational force is in the negative y-direction. This problem has been extensively studied by finite element methods (FEM) [3, 50] and LBE methods [13, 39, 51, 52]. To mimic an infinite channel, a
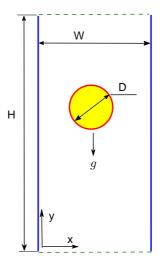
Figure 3: The schematic diagram for a circular particle settling under gravity in an infinite channel.

moving computational domain is used in these methods to capture the relevant section of the infinite domain, which is also adopted in our simulations.

In simulations, the relaxation rates in the MRT scheme are set as follows: $s_0 = s_3 = s_5 = 0$ for the conserved moments, $s_7 = s_8 = 1/\tau$ are determined by the shear viscosity ν based on Eq. (2.15), while other relaxation rates are determined by the linear stability analysis [45, 47, 48]. In our simulations, they are specified to be $s_4 = s_6 = 1.8$, and $s_1 = 1.1$, $s_2 = 1.25$ unless otherwise stated. For consistency, in Ladd's scheme, we set $\lambda_\zeta = 4s_1/(s_1 - 6)$ so that the bulk viscosity is identical to that of the MRT scheme.

3.1 Accuracy

At low Reynolds numbers, an approximate analytical solution for the drag force on the circular particle between two infinite and parallel walls can be expressed as [53]

$$\boldsymbol{F}_d = 4\pi K \mu \boldsymbol{U}, \tag{3.1}$$

where $\boldsymbol{U}$ is the settling velocity of the particle, μ is the dynamic viscosity of the fluid, and K is a wall correction factor that reflects the effect of the channel walls on the drag force

$$K = \frac{1}{\ln W^* - 0.9157 + 1.7244(W^*)^{-2} - 1.7302(W^*)^{-4} + 2.4056(W^*)^{-6} - 4.5913(W^*)^{-8}}, \tag{3.2}$$

where $W^* = W/D$. When the particle is settling vertically at the constant speed, the gravity force and the buoyancy force are balanced. The drag force can thus be given as

$$\boldsymbol{F}_d = \frac{1}{4}\pi D^2 (\rho_f - \rho_s)\boldsymbol{g}, \tag{3.3}$$

where g is the gravitational acceleration, and ρ_s and ρ_f are the particle density and fluid density, respectively. So, the terminal sedimentation velocity of the particle is:

$$\boldsymbol{U}_t = \frac{D^2}{16K\mu}(\rho_f - \rho_s)\boldsymbol{g} = \frac{D^2}{16K\nu}(1 - \rho_r)\boldsymbol{g}, \tag{3.4}$$

where $\rho_r = \rho_s/\rho_f$ is the ratio of particle to fluid densities, and $\nu = \mu/\rho_f$ is the kinematic viscosity of the fluid. With this analytical solution, we can evaluate the accuracy of the three LBE schemes.

The test problem has been studied by Nie et al. [39] using a LBE method coupled with a direct-forcing fictitious domain technique [54] (LB-DF/FD). For comparison, the computational parameters in the present simulation are taken the same as those used in [39]. The computational domain is $W \times H = 1.2cm \times 6cm$, the diameter of the particle is $D = 0.24cm$, the density and viscosity of the fluid are set to be $\rho_f = 1.0g/cm^3$ and $\mu = 0.1g/(cm \cdot s)$, respectively. A lattice with size of 120×600 is used to cover the computation domain, and the relaxation time τ related to the shear viscosity is set to be 0.8. Initially, the particle is located at $(0.6cm, 3.0cm)$ and held at rest (same as the fluid), and the gravity accelerating velocity is $g = 980.0cm/s^2$. In our simulations, zero velocities are applied uniformly at the inflow boundary which is always $12.5D$ from the moving particle, and the normal derivative of velocity is set to be zero at the outflow boundary which is $12.5D$ from the particle. These boundary conditions are the same as those used in [12, 13, 39]. No-slip boundary conditions are applied to the left and right walls, and the non-equilibrium extrapolation scheme [55] is used to treat the boundary conditions at the inlet and outlet. In our simulations, a moving mesh technique [39] is adopted so that the computational domain moves with the particle. The technique of treatment is briefly as follows: If the particle moves downward by one lattice unit, one layer of fluid nodes at the downstream side is removed from the grid system and one layer of lattice nodes will be added to the upstream side.

A number of tests with different density ratios ρ_r and Reynolds numbers Re_p are carried out. Here the particle Reynolds number Re_p is defined by $Re_p = \rho_f U_c D/\mu$, where U_c is the speed of the terminal settling velocity of the particle. In Fig. 4, the velocities from the three LBE schemes are shown together with the analytical and the simulation results in [39]. Also the corresponding particle Reynolds number (Re_p) are listed in the blankets. It is clear that the results obtained by the three LBE schemes are well consistent with that by the LB-DF/FD method [39], except for the case of $\rho_r = 0.95$. In this case, the particle velocities predicted by the BGK and Ladd's schemes deviate sharply from the constant terminal velocity as time marches to $t > 2.1s$, while the result of the MRT scheme is still satisfactory. This is not surprising since Ladd's (and the LBGK) scheme has a requirement that $\rho_s/\rho_f > 1$. This fact indicates that the MRT scheme may release this constraint. Fig. 4 also shows that the LBE results deviate from the analytical solutions given by Eq. (3.4) as $|\rho_r - 1|$ becomes larger. This may be because Eq. (3.4) is valid only for small Reynolds numbers [53].
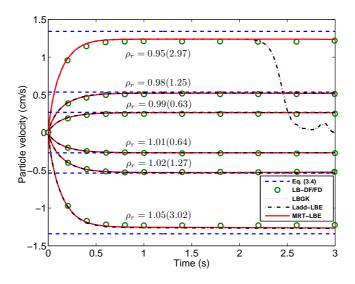
Figure 4: Comparison of the vertical velocities of the particle during sedimentation at $W/D=5$ for different particle densities. The open circles are the results obtained by the LB-DF/FD method from [39], and the dashed lines are analytical solutions obtained from Eq. (3.4). The number in the blanket of each case is the particle Reynolds number.

In addition, we also conduct simulations using the MRT scheme with another set of relaxation parameters: $s_1 = 1.1$, $s_2 = 1.0$, $s_4 = s_6 = 1.2$, and other relaxation parameters are set to remain unchanged. It is found that the results are very close. For example, in the case of $\rho_r = 0.95$, the magnitude of the terminal velocity of the particle obtained from the two sets of relaxation parameters are respectively $1.2324 cm/s$ and $1.2380 cm/s$, with a relative error within 0.454%.

We also noticed that there exist some slight differences between the magnitudes of the simulating velocities for $\rho_r = 1 + \alpha$ and $\rho_r = 1 - \alpha$, although they should be theoretically identical as given by Eq. (3.4). This may be due to the effects of the interior fluid in the particle adopted in the present method. However, the difference is very small. For example, the largest difference is 3.05% between the velocity magnitudes for the cases of $\rho_r = 0.95$ and 1.05.

As noted previously, Ladd's scheme can be viewed as a special case of the MRT scheme ($s_1 = 6\lambda_\zeta / (\lambda_\zeta - 4)$, $s_7 = s_8 = -\lambda_\nu$, and other $s_i = 1.0$). We will demonstrate this point numerically. In Fig. 5 the time history of the particle velocity predicted by the MRT-LBE and Ladd's scheme are shown. One can observe that the results from the two schemes are nearly indistinguishable. To quantify the differences, we measure the relative difference of the velocity:

$$E(t) = \frac{|\boldsymbol{U}_{pL}(t) - \boldsymbol{U}_{pM}(t)|}{|\boldsymbol{U}_{pM}(t)|}, \tag{3.5}$$

where $\boldsymbol{U}_{pL}(t)$ and $\boldsymbol{U}_{pM}(t)$ represent the instantaneous settling velocity of the particle obtained by Ladd's scheme and MRT scheme, respectively. The time history of relative
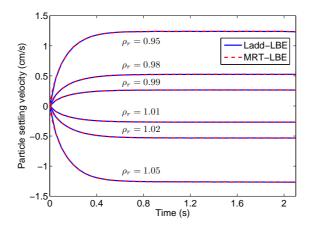
Figure 5: Particle settling velocity at different density ratios predicted by the MRT and Ladd's schemes ($s_1 = 6\lambda_\zeta/(\lambda_\zeta-4)$, $s_7=s_8=-\lambda_\nu$, and other relaxation rates are set to be 1.0).

difference is plotted in Fig. 6(a) for $\rho_r < 1$ and Fig. 6(b) for $\rho_r > 1$. It can be seen that the difference of the instantaneous velocities between the two schemes are very small (within 0.1%) in all of the cases considered. These results indicate that Ladd's scheme can indeed be regarded as a special case of the MRT scheme.
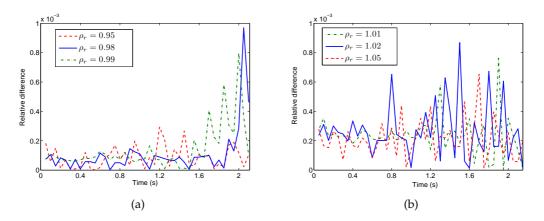

Figure 6: Time variation of relative difference of particle settling velocity computed with Ladd's scheme and the present MRT scheme.

3.2 Numerical stability and computational efficiency

We now focus on the numerical stability of the three schemes. In our study, the stability can be characterized by the minimum value of τ (τ_{min}) below which numerical instability will appear. It is hard to determine the exact τ_{min} numerically, and we will roughly obtain it by increasing from $\tau=0.5$ with a small increment ς. A set of simulations are conducted

Table 1: τ_{min} with different grid resolution ($\rho_s = 1.01g/cm^3$).

	τ_{min}		
D/δ_x	LBGK	Ladd-LBE	MRT-LBE
10	1.3805	1.2285	1.1575
24	0.7505	0.7235	0.6895
40	0.5405	0.5345	0.5270
60	0.5255	0.5200	0.5120

Table 2: CPU time(s) of running 10000 time steps for the three LBE schemes.

		Scheme		
D/δ_x	τ	LBGK	Ladd-LBE	MRT-LBE
24	0.8	147.48	166.30	167.63
	1.0	142.39	166.88	167.78
	1.2	148.42	167.25	168.58
	1.6	150.61	169.34	170.19
	2.0	145.66	170.38	170.78
Maximum time increase			17.2%	17.83%
48	0.8	574.41	649.33	653.98
	1.0	550.72	649.76	654.00
	1.2	578.95	649.94	656.95
	1.6	580.06	655.50	658.11
	2.0	561.66	658.27	657.61
Maximum time increase			17.98%	18.75%

with different grid resolutions, and the computation is said to be stable if it works stably till $t = 5.0s$. ς is set to be 5×10^{-4} in our tests. Table 1 lists the values of τ_{min} for the three models with different lattices. The results given in Table 1 make it clear that the MRT scheme is the most stable one among the three schemes on each mesh, while the LBGK is the worst. Furthermore, it is found that the value of τ_{min} decreases with decreasing δ_x for each schemes.

We next pay our attention to the computational efficiency of the three LBE schemes. To make a quantitative comparison, we used two different grid meshes, i.e., $D = 24\delta_x$ and $D = 48\delta_x$ with different values of τ. For the parameter λ_ζ in the Ladd's scheme and other relaxation rates in the MRT scheme, they are chosen as those described at the beginning of this section. In all of these simulations, the particle-to-fluid density ratio ρ_r is fixed at 1.01, and the particle diameter D is chose to be $0.24cm$. With the aid of Intel(R) C++ compiler 9.0, our simulations were conducted on a dual core Intel(R) E2180, CPU 2.00GHz. Table 2 lists the CPU time for running 10000 time steps. As expected, it is found that the BGK scheme takes the least CPU time, while the computation times of Ladd's scheme and the MRT scheme are almost the same although the former is slightly

faster. It is also seen that both the MRT scheme and Ladd's scheme are approximately $15\sim20\%$ slower than the BGK scheme. Overall, we can make a descending order with respect to the computational efficiency of these three different schemes as follows: the BGK scheme, Ladd's scheme, and the MRT scheme.

3.3 Robustness

In the sedimentation process of a particle in an infinite channel, the particle is dragged to move and rotate in response to hydrodynamic and gravitational forces. The channel walls have significant effects on the particle, and the effects can be described by the wall correction factor K given by Eq. (3.2). As shown, K depends only on the geometric parameter and irrelative to fluid properties such as the viscosity. In this section, we will test the robustness of the three LBE schemes by measuring the wall correction factor with different values of τ.

The wall correction factor K can be derived analytically from Eq. (3.4) and explicitly written as follows:
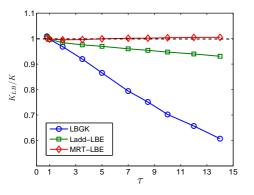
$$K = \frac{D^2(1-\rho_r)g}{16\nu U_c},\tag{3.6}$$

where U_c is the speed of the terminal settling velocity of the particle which can be measured from the simulations, and g is the magnitude of the acceleration of gravity. In our simulation, the following relaxation parameters of the MRT scheme will be employed:

$$s_1 = s_2 = s_7 = s_8 = 1/\tau, \quad s_4 = s_6 = 8\frac{(2-s_8)}{(8-s_8)}.\tag{3.7}$$

Substantially, Eq. (3.7) gives only two different relaxation rates in response to the even-order and odd-order modes of the MRT scheme [23]. s_7 is the relaxation rate for the even-order modes which is determined by the shear viscosity according to Eq. (2.15), while s_4 is the relaxation rate for the odd-order modes given by Eq. (3.7) so that the actual location where the no-slip boundary conditions are satisfied is viscosity independent [23,56,57]. Furthermore, Eq. (3.7) has been also adopted in [58], where Pan *et al.* applied such set of relaxation parameters to study the viscosity-dependent permeability in porous media simulation. For Ladd's scheme, the two parameters λ_ν and λ_ζ are set as before. The acceleration of gravity is afresh set to be $g = 0.1 cm/s^2$ in the simulations, and τ is varied from 0.8 to 14.0. The density ratio is specified to be $\rho_r = 1.01$, and the diameter of the particle is $D = 0.24 cm$. The particle size is first chosen to be 24 lattice units, which is sufficiently accurate for computations.

The normalized wall correction factor, $K^* = K_{LB}/K$, where K_{LB} is measured from the LBE simulations according to Eq. (3.6) and K is given by Eq. (3.2), are plotted in Fig. 7 as a function of τ. As can be seen from the figure, for the LBGK scheme K^* decreases almost linearly with the relaxation time τ in the case of $D = 24\delta_x$, which is unphysical. For Ladd's scheme, the computed K^* also decreases linearly, but with a smaller rate compared with the LBGK scheme. Contrary to the LBGK and Ladd's schemes, K^* predicted
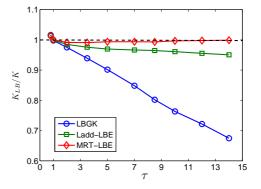
Figure 7: The normalized wall correction factor K^* versus the relaxation time τ with $g=0.1$ and $D=24\delta_x$.

Figure 8: Same as Fig. 7 at $D=32\delta_x$.

by the MRT scheme exhibits an almost unchanged value in the whole range of τ. We also test this property with a finer grid ($D=32\delta_x$), and similar tendency is observed (Fig. 8). These results clearly show that the MRT scheme is the most robust one among the three schemes.

4 Numerical results of the sedimentation of an elliptical particle

In this section, we will perform some numerical simulations of the sedimentation of an elliptical particle in an infinite channel to further compare the three LBE schemes. Many studies of this problem have been reported [13, 14, 60]. As shown by Feng et al. [3] and Huang et al. [59], the sedimenting elliptical particle can behave much differently from a circular one due to its orientation.

In the following simulations, we will adopt the same computational conditions as used by Xia et al. [60], who used both a FEM and a multi-block LBE method to solve the two-dimensional problem. The elliptical particle is initially located at the center of a two-dimensional channel with a width of $W=0.4cm$, and the orientation angle of the particle with the horizontal axis is $\theta=\pi/4$, as depicted in Fig. 9. The major and minor axes of the ellipse are $a=0.1cm$ and $b=0.05cm$, respectively. The lattice spacing is $\delta_x=1/260cm$. The fluid density is $\rho_f=1.0g/cm^3$, and its kinematic viscosity is $\mu=0.01cm^2/s$. The elliptical particle is heavier than the fluid and settles under gravity acting in the negative y-direction. To simulate the motion of the particle in an infinite channel, the moving mesh method is again used here. Zero velocity condition (no-flow condition) is imposed at the inflow boundary which is kept at a distance of $15a$ ahead of the center of the ellipse, while the fully developed flow condition is applied to the outflow boundary which is $25a$ behind the ellipse.

In Fig. 10, we compare the particle's vertical velocities predicted by the three LBE schemes with $\tau=0.648$ together with that computed using the FEM [60] when the particle-
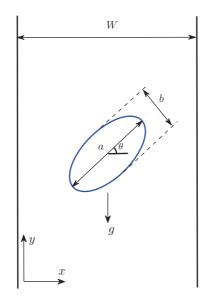
Figure 9: Schematic of the sedimentation of an elliptical particle in an infinite channel.

fluid density ratio $\rho_r = \rho_s/\rho_f = 1.1$. The particle Reynolds number Re_p based on the terminal velocity and the major axis of the particle is 12.78. As depicted in the figure, after a period of sedimentation, the vertical velocity profiles of the ellipse obtained by the BGK and Ladd's scheme successively and obviously deviate from the finite-element result [60], the velocity predicted by the BGK scheme exhibits some strong oscillations, and that obtained by Ladd's scheme also shows some oscillations weaker than that of the BGK scheme. Such oscillations can lead to numerical instability as τ is further decreased. On the contrary, the velocity computed by the MRT scheme agrees quite well with the element-finite result and no oscillations appear. These results indicate that the MRT scheme can provide much satisfied numerical results and better numerical stability as compared with the other two LBE schemes. To strengthen this point, we further decrease τ to 0.60 and increase Re_p to a larger value by increasing ρ_r from 1.1 to 1.3. It is found that the vertical settling velocity computed by the BGK scheme and Ladd's scheme deviates from the reference result with significant oscillations, whereas the MRT scheme still works well and gives reliable results that are consistent with the finite-element result [60] (Fig. 11). Additionally, it is found that the MRT scheme is slower than the BGK and Ladd's scheme in terms of the computational efficiency, as observed in Section 3.2.

Also, different to the BGK scheme and Ladd's scheme, for the two density ratios ρ_r the velocity profiles of the elliptical particle predicted by the MRT scheme are in excellent agreement with the FEM results [60], as clearly shown in Figs. 10 and 11. This indicates that the results computed by the MRT scheme are less sensitive in comparison with the other two schemes. These results further demonstrate the better robustness of the MRT scheme.
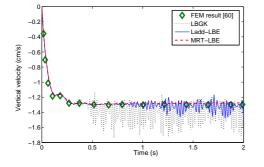
Figure 10: Comparison of the vertical settling velocity obtained by the three LBE schemes at $\tau = 0.648$ with the finite-element result of Xia et al. [60] for an elliptical particle as $\rho_r = 1.1$.
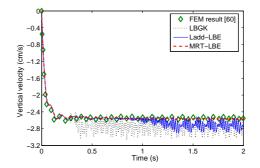
Figure 11: Same as Fig. 10 at $\tau = 0.60$ as $\rho_r = 1.3$.

5 Conclusions

In this work, we present a comparative study among three LBE schemes, i.e., the BGK model, Ladd's model, and the MRT model. The sedimentation of a circular and an elliptical particle in a two-dimensional infinite channel under gravity are used as the test problems. The accuracy, numerical stability, computational efficiency, and robustness of the three schemes are carefully analyzed in the simulations of sedimentation of a circular particle. Our main results are summarized as follows.

First, the sedimentation velocities predicted by the three schemes agree well with the analytical and available data in general in the six cases of density ratios, except that in the case of $\rho_r=0.95$ the particle velocities obtained by both the BGK scheme and Ladd's scheme deviate from the other results at later stage. It is also observed that with properly chosen relaxation times, the MRT scheme and Ladd's scheme produces nearly identical results, which confirms that Ladd's scheme is also a special case of the MRT scheme, just like the LBGK scheme. In this regard, the MRT scheme is the most general model for simulations of particulate flows. Second, the numerical stability of the three LBE schemes are investigated by comparing the minimum values of the reachable relaxation time for the shear viscosity. It is found that the MRT scheme is the most stable scheme while the LBGK scheme is the worst. However, the LBGK scheme is the most efficient one in terms of the CPU times, while the MRT and Ladd's schemes are nearly identical (with about $15 \sim 20\%$ increase in comparison with the LBGK scheme). Third, the robustness of the three LBE schemes are also investigated. It is found that in the case of $D = 24\delta_x$ the normalized values of wall correction factor K^* computed by both the LBGK scheme and Ladd's scheme show a linear decrease with the relaxation time, although the decrease rate of K^* of Ladd's scheme is smaller than that of the BGK scheme. On the contrary, the MRT scheme gives almost a fixed value of K^*. In addition, these three LBE schemes produce such similar results in another case of $D = 32\delta_x$.

In the test problem of the sedimentation of an elliptical particle, the numerical results

computed by the three LBE schemes are also compared. It is again found that the MRT scheme can provide more accurate results and better numerical stability than the BGK and Ladd's scheme. Although the computational cost of the MRT scheme is the largest, we would like to point out that it is more robust and insensitive.

These results show that the MRT scheme is a good choice for particulate flows since it can achieve better accuracy, numerical stability, and robustness than the other two schemes, which are demonstrated in our simulations.

Acknowledgments

References

[1] Y. C. Fung, Biomechchanics Circulation, Springer-Verlag, Berlin, 1997.
[2] D. E. Smith, H. P. Babcock and S. Chu, Single-polymer dynamics in steady shear flow, Science, 283 (1999), 1724-1727.
[3] J. Feng, H. H. Hu and D. D. Joseph, Direct simulation of initial value problems for the motion of solid bodies in a Newtonian fluid: Part 1. Sedimentation, J. Fluid Mech., 261 (1994), 95-134.
[4] J. Feng, H. H. Hu and D. D. Joseph, Direct simulation of initial value problems for the motion of solid bodies in a Newtonian fluid: Part 2. Couette and Poiseuille flows, J. Fluid Mech., 277 (1994), 271-301.
[5] N. A. Patankar and D. D. Joseph, Lagrangian numerical simulation of particulate flows, Int. J. Multiphase Flow, 27 (2001), 1685-1706.
[6] N. A. Patankar and D. D. Joseph, Modeling and numerical simulation of particulate flows by the Eulerian-Lagrangian approach, Int. J. Multiphase Flow, 27 (2001), 1659-1684.
[7] R. Benzi, S. Succi and M. R. Vergassola, The lattice Boltzmann equation: theory and applications, Phys. Rep., 222 (1992), 145-197.
[8] S. Y. Chen and G. D. Doolen, Lattice Boltzmann method for fluid flows, Annu. Rev. Fluid Mech., 30 (1998), 329-364.
[9] S. Succi, The Lattice Boltzmann Equation for Fluid Dynamics and Beyond, Oxford University Press, New York, 2001.
[10] A. J. C. Ladd, Numerical simulations of particulate suspensions via a discretized Boltzmann equation, Part I. Theoretical foundation, J. Fluid Mech., 271 (1994), 285-310.
[11] A. J. C. Ladd, Numerical simulations of particulate suspensions via a discretized Boltzmann equation, Part II. Numerical results, J. Fluid Mech., 271 (1994), 311-339.
[12] C. K. Aidun and Y. N. Lu, Lattice Boltzmann simulation of solid particles suspended in fluid, J. Stat. Phys., 81 (1995), 49-61.
[13] C. K. Aidun, Y. N. Lu and E. J. Ding, Direct analysis of particulate suspensions with inertia using the discrete Boltzmann equation, J. Fluid Mech., 373 (1998), 287-311.

[14] D. W. Qi, Lattice-Boltzmann simulations of particles in non-zero-Reynolds-number flows, J. Fluid Mech., 385 (1999), 41-62.

[15] Z. G. Feng and E. E. Michaelides, Interparticle forces and lift on a particle attached to a solid boundary in suspension flow, Phys. Fluids, 14 (2002), 49-60.

[16] A. J. C. Ladd and R. Verberg, Lattice-Boltzmann simulation of particle-fluid suspensions, J. Stat. Phys., 104 (2001), 1191-1125.

[17] Z. G. Feng and E. E. Michaelides, Robust treatment of no-slip boundary condition and velocity updating for the lattice-Boltzmann simulation of particulate flows, Comput. Fluids, 38 (2009), 370-381.

[18] J. S. Wu and C. K. Aidun, Simulating 3D deformable particle suspensions using lattice Boltzmann method with discrete external boundary force, Int. J. Numer. Meth. Fluids, 62 (2010), 765-783.

[19] E. Lorenz, A. Caiazzo and A. G. Hoekstra, Corrected momentum exchange method for lattice Boltzmann simulations of suspension flow, Phys. Rev. E, 79 (2009), 036705.

[20] T. Inamuro, M. Yoshino and F. Ogino, A non-slip boundary conditions for lattice Boltzmann simulation, Phys. Fluids, 7 (1995), 2928-2930.

[21] R. Mei, D. Yu, W. Shyy and L. S. Luo, Force evolution in the lattice Boltzmann method involving curved geometry, Phys. Rev. E, 65 (2002), 041203.

[22] P. Lallemand and L. S. Luo, Lattice Boltzmann method for moving boundaries, J. Comput. Phys., 184 (2003), 406-421.

[23] I. Ginzburg and D. d'Humières, Multireflection boundary conditions for lattice Boltzmann models, Phys. Rev. E, 68 (2003), 066614.

[24] A. ten Cate, C. H. Nieuwstad, J. J. Derksen and H. E. A. Van den Akker, Particle imaging velocity experiments and lattice-Boltzmann simulations on a single sphere settling under gravity, Phys. Fluids, 14 (2002), 4012-4025.

[25] D. R. J. Owen, C. R. Leonardi and Y.T. Feng, An efficient framework for fluidCstructure interaction using the lattice Boltzmann method and immersed moving boundaries, Int. J. Numer. Meth. Eng, 87 (2011), 66-95.

[26] S. Kollmannsberger, S. Geller, J. Düster A, Tölke, C. Sorger, M. Krafczyk and E. Rank, Fixed-grid fluid-structure interaction in two dimensions based on a partitioned Lattice Boltzmann and p-FEM approach, Int. J. Numer. Meth. Eng, 79 (2009), 817-845.

[27] Y. T. Feng, K. Han and D. R. J Owen, Coupled lattice Boltzmann method and discrete element modelling of particle transport in turbulent fluid flows: Computational issues, Int. J. Numer. Meth. Eng, 72 (2007), 1111-1134.

[28] Y. T. Feng, K. Han and D. R. J. Owen, Combined three-dimensional lattice Boltzmann methods and discrete element method for modeling fluid-particle interactions with experiment assessment, Int. J. Numer. Meth. Eng, 81 (2010), 229-245.

[29] C. S. Peskin, Numerical analysis of blood flow in the heart, J. Comput. Phys., 25 (1977), 220-252.

[30] C. S. Peskin, The immersed boundary method, Acta Numer., 11 (2002), 479-517.

[31] Z. G. Feng and E. E. Michaelides, The immersed boundary-lattice Boltzmann method for solving fluid-particles interaction problem, J. Comput. Phys., 195 (2004), 602-628.

[32] Z. G. Feng and E. E. Michaelides, Proteus: a direct forcing method in the simulations of particulate flows, J. Comput. Phys., 202 (2005), 20-51.

[33] X. D. Niu, C. Shu, Y. T. Chew and Y. Peng, A momentum exchange-based immersed boundary-lattice Boltzmann method for simulating incompressible viscous flows, Phys. Lett. A, 354 (2006), 173-182.

[34] J. Wu and C. Shu, Particulate flow simulation via a boundary condition-enforced immersed boundary-lattice Boltzmann scheme, Commun. Comput. Phys., 7 (2010), 793-812.

[35] B. K. Cook, D. R. Noble and J. R. Williams, A direct simulation method for particle-fluid systems, Eng. Computation, 21 (2004), 151-168.

[36] X. Shi and S. P. Lim, A LBM-DLM/FD method for 3D fluid-structure interactions, J. Comput. Phys, 226 (2007), 2028-2043.

[37] M. Rohde, J. J. Derksen and H. E. A. van der Akker, An applicability study of advanced lattice-Boltzmann techniques for moving, no-slip boundaries and local grid refinement, Comput. Fluids, 37 (2008), 238-1252.

[38] A. Dupuis, P. Chatelain and P. Koumoutsakos, An immersed boundary-lattice-Boltzmann method for the simulation of the flow past an impulsively started cylinder, J. Comput. Phys, 227 (2008), 4486-4498.

[39] D. M. Nie and J. Z. Lin, A LB-DF/FD method for particle suspension, Commun. Comput. Phys., 7 (2010), 544-563.

[40] Y. Peng and L. S. Luo, A comparative study of immersed-boundary and interpolated bounce-back methods in LBE, Prog. Comput. Fluid Dyna., 8 (2008), 156-167.

[41] R. G. M. van der Sman, MRT Lattice Boltzmann schemes for confined suspension flows, Comput. Phys. Commun., 181 (2010), 1562-1569.

[42] Y. H. Qian, D. d'Humières and P. Lallemand, Lattice BGK models for Navier-Stokes equation, Europhys. Lett., 17 (1992), 479-484.

[43] H. Chen, S. Chen and W. Matthaeus, Recovery of the Navier-Stokes equations through a lattice gas Boltzmann equation method, Phys. Rev. A, 45 (1992), 5339-5342.

[44] U. Frisch, D. d'Humières, B. Hasslacher, P. Lallemand, Y. Pomeau and J.-P. Rivet, Lattice gas hydrodynamics in two and three dimensions, Complex Syst., 1 (1987), 649-707.

[45] P. Lallemand and L.S. Luo, Theory of the lattice Boltzmann method: Dispersion, dissipation, isotropy, Galilean invariance, and stability, Phys. Rev. E, 61 (2000), 6546-6562.

[46] D. d'Humières, Generalized lattice-Boltzmann equations, In: Shizgal D et al., editors. RGD, Prog. Astronaut. Aeronaut 159 (1992), 450-458.

[47] D. d'Humières, I. Ginzburg, M. Krafczyk, P. Lallemand, L. S. Luo, Multiple-relaxation-time lattice Boltzmann models in three-dimensions, Phil. Trans. R. Soc. A, 360 (2002), 437-51.

[48] P. Lallemand and L-S. Luo, Theory of the lattice Boltzmann method: acoustic and thermal properties in two and three dimensions, Phys. Rev. E, 68 (2003), 036706.

[49] D. Wan and S. Turek, Direct numerical simulation of particulate flow via multigrid FEM techniques and the fictitious boundary method, Int. J. Numer. Meth. Fluids, 51 (2006), 531-566.

[50] H. H. Hu, D. D. Joseph and M. J. Crochet, Direct simulation of fluid particle motions, Theo. Comput. Fluid Dyn., 3 (1992), 285-306.

[51] H. B. Li, X. Y. Lu, H. P. Fang and Y. H. Qian, Force evolution in lattice Boltzmann simulations with moving boundaries in two dimensions, Phys. Rev. E, 70 (2004), 026701.

[52] O. E. Strack and B. K. Cook, Three-dimensional immersed boundary conditions for moving solids in the lattice-Boltzmann method, Int. J. Numer. Meth. Fluids, 55 (2007), 103-125.

[53] J. Happel and H. Brenner, Low Reynolds Number Hydrodynamics, Prentice-Hall, New York, 1965.

[54] Z. S. Yu and X. M. Shao, A direct-forcing fictitious domain method for particulate flows, J. Comput. Phys., 227 (2007), 292-314.

[55] Z. L. Guo, C. G. Zheng and B. C. Shi, An extrapolation method for boundary conditions in lattice Boltzmann method, Phys Fluids, 14 (2007), 2007-2010.

[56] I. Ginzburg and P. Adler, Boundary flow condition analysis for the three-dimensional lattice Boltzmann model, J. Phys., II 4 (1994), 191-214.

[57] I. Ginzburg and D. d'Humières, Local second-order boundary methods for lattice Boltzmann models, J. Stat. Phys, 84 (1996), 927-971.

[58] C. Pan, L. S. Luo and C. T. Miller, An evaluation of lattice Boltzmann schemes for porous medium flow simulation, Comput. Fluid, 35 (2006), 898-909.

[59] P. Huang, H. Hu, and D. Joseph, Direct simulation of the sedimentation of elliptic particles in Oldroyd-b fluids, J. Fluid Mech., 362 (1998), 297-325.

[60] Z. H. Xia, K. W. Connington, S. Papaka, P. T. Yue, J. J. Feng and S. Y. Chen, Flow patterns in the sedimentation of an elliptical particle, J. Fluid Mech., 625 (2009), 249-272.